Stereochemical Control of Small Molecule Binding to Bulged DNA: Comparison of Structures of Spirocyclic Enantiomer-Bulged DNA Complexes[†,‡]

Geum-Sook Hwang,[§] Graham B. Jones,[||] and Irving H. Goldberg*[,§]

Department of Biological Chemistry and Molecular Pharmacology, Harvard Medical School, Boston, Massachusetts 02115, and Bioorganic and Medicinal Chemistry Laboratories, Department of Chemistry, Northeastern University, Boston, Massachusetts 02115

Received October 8, 2003; Revised Manuscript Received November 24, 2003

ABSTRACT: The solution structure of the complex formed between an oligonucleotide containing a two-base bulge (5′-CACGCAGTTCGGAC•5′-GTCCGATGCGTG) and ent-DDI, a designed synthetic agent, has been elucidated using high-resolution NMR spectroscopy and restrained molecular dynamic simulation. Ent-DDI is a left-handed wedge-shaped spirocyclic molecule whose aglycone portion is an enantiomer of DDI, which mimicks the spirocyclic geometry of the natural product, NCSi-gb, formed by base-catalyzed activation of the enediyne antibiotic neocarzinostatin. The benzindanone moiety of ent-DDI intercalates between the A6•T21 and the T9•A20 base pairs, overlapping with portions of the purine bases; the dihydronaphthalenone moiety is positioned in the minor groove along the G7-T8-T9 bulge sequence; and the aminoglycoside is in the middle of the minor groove, approaching A20 of the nonbulged strand. This alignment of ent-DDI along the DNA helical duplex is in the reverse direction to that of DDI. The aminoglycoside moiety of ent-DDI is positioned in the 3′ direction from the bulge region, whereas that of the DDI is positioned in the 5′ direction from the same site. This reverse binding orientation within the bulge site is the natural consequence of the opposite handedness imposed by the spirocyclic ring junction and permits the aromatic ring systems of the two spirocyclic enantiomers access to the bulge region. NMR and CD data indicate that the DNA in the DDI-bulged DNA complex undergoes a larger conformational change upon complex formation in comparison to the ent-DDI-bulged DNA, explaining the different binding affinities of the two drugs to the bulged DNA. In addition, there are different placements of the bulge bases in the helical duplex in the two complexes. One bulge base (G7) stacks inside the helix, and the other one (T8) is extrahelical in the DDI-bulged DNA complex, whereas both bulge bases in the ent-DDI-bulged DNA complex prefer extrahelical positions for drug binding. Elucidation of the detailed binding characteristics of the synthetic spirocyclic enantiomers provides a rational basis for the design of stereochemically controlled drugs for bulge binding sites.

Bulged sites in DNA are not only crucial structural elements for the recognition by DNA repair proteins (*1*−*3*) but also exhibit remarkable affinities for drug interactions. The interaction of drug molecules at bulge sites has been of considerable interest since binding at these sites has the potential to stabilize and increase the lifetime of the bulge state and its propensity to induce frameshift mutations and DNA strand slippage synthesis. It has already been demonstrated that intercalators, such as ethidium bromide, 9-aminoacridine, and a number of antitumor antibiotics have increased binding affinity for sites on duplex DNA carrying a single-base bulge (*4*−*7*). Of special interest, the enediyne antitumor antibiotic neocarzinostatin (NCS-chrom)[1] induces highly efficient site-specific strand cleavage at either single- or two-base bulges depending on the particular mode of activation of the drug (*7*−*9*). In other cases, chemical modification of DNA and RNA by drugs appears to occur primarily near bulge sites because of better binding site access (*10*), while selective drug binding to RNA bulges has been shown to inhibit protein−RNA recognition (*11*) and to result in specific cleavage at the bulge site (*12*).

We have designed a number of spirocyclic model compounds with specific affinity for bulged sites (two unpaired bases) in DNA based on our earlier work with NCS-chrom

[†] This research was supported by U.S. Public Health Services Grants GM 53793 to I.H.G. and GM 57123 to G.B.J. from the National Institute of Health.

[‡] The structures have been deposited in the RCSB Protein Data Bank (1R4E).

* To whom correspondence should be addressed. Tel: (617) 432-1787. Fax: (617) 432-0471. Email: irving_goldberg@hms.harvard.edu.

[§] Harvard Medical School.

[||] Northeastern University.

[1] Abbreviations: 1-D, one-dimensional; 2-D, two-dimensional; BI, benzindanone; CNS, crystallography and NMR system; DDI, double decker intercalator; ent-DDI, spirocyclic (aglycone) enantiomer of DDI; DG, distance geometry; DQF−COSY, double quantum filtered correlation spectroscopy; EDTA, ethylenediaminetetraacetic acid; HPLC, high performance liquid chromatography; NCS, neocarzinostatin; NCS-chrom, native form of NCS chromophore; NCSi-gb, post-activated NCS-chrom formed under base-catalyzed conditions; NMF, 2-*N*-methylfucosamine; NMR, nuclear magnetic resonance; NA, dihydronaphthone; NAP, dihydronaphthalenone; nucleic acids: A: adenosine, C: cytidine, G: guanosine, T: thymidine; NOE, nuclear Overhauser effect; NOESY, nuclear Overhauser effect and exchange spectroscopy; RMSD, root-mean-square deviation; THI, tetrahydroindacene; TOCSY, total correlation spectroscopy.

10.1021/bi035824i CCC: $27.50
Published on Web 12/31/2003

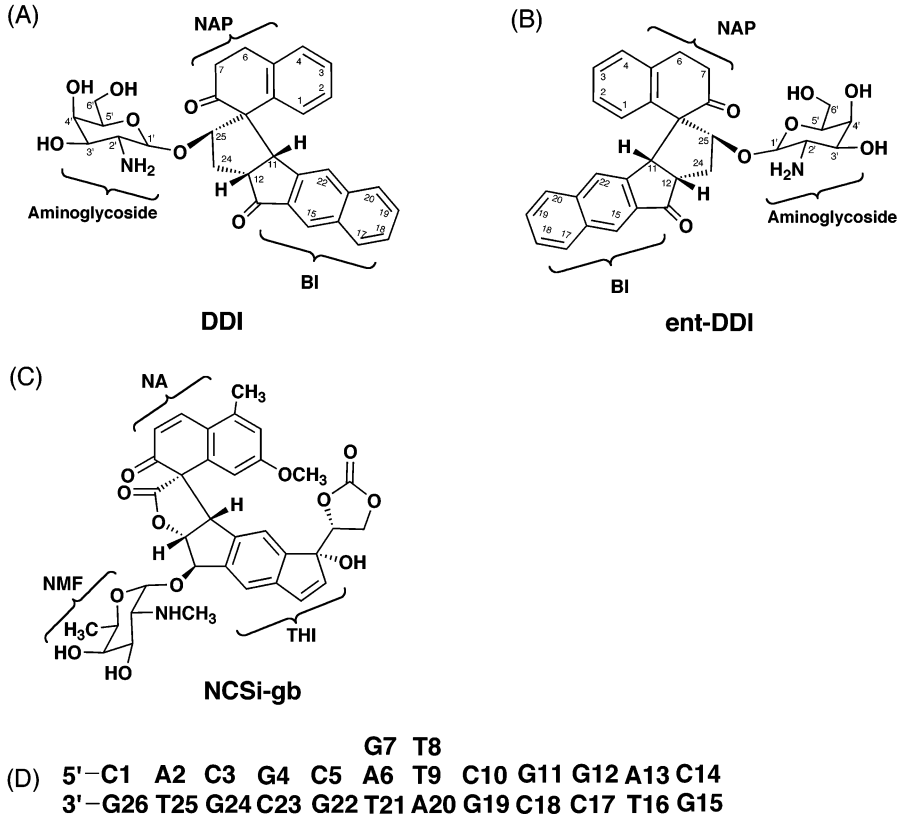

FIGURE 1: Chemical structures of the synthesized spirocyclic agents (A) DDI and (B) ent-DDI; (C) natural product, NCSi-gb; and (D) sequence of the bulged DNA duplex consisting of 12-mer nonbulged and 14-mer bulged strands.

(*13*, *14*). NCS-chrom undergoes general base-catalyzed activation to a biradical species that selectively cleaves nucleic acids at bulged sites having two unpaired bases (*14*). In the absence of a bulged DNA target, a wedge-shaped spirocyclic molecule (NCSi-gb) (Figure 1C) is generated that resembles the DNA cleaving species and binds to the bulged site with great specificity (*15*, *16*). On the basis of a structural study of the complex formed between NCSi-gb and oligodeoxynucleotide possessing a target bulge site (*17*, *18*), we have been able to determine that the important feature responsible for bulge binding is the spirocyclic structure consisting of two aromatic ring systems fixed in relation to each other by a connecting spirocyclic ring, to form a wedge-shaped molecule. In the synthesis of analogues of NCSi-gb, we obtained two spirocyclic agents whose structures have an enantiomeric relationship (*19*, *20*). The spirocyclic enantiomers were converted to diastereomers after addition of an aminosugar moiety (Figure 1A,B). The spirocyclic geometry of DDI (Figure 1A) mimicks that of the natural product, NCSi-gb, in having two aromatic ring systems with a right-handed twist angle (~35°) at the spirocyclic ring junction, whereas the geometry of the spirocyclic enantiomer ent-DDI (Figure 1B) is an inverted form with a left-handed twist angle (*20*). DDI and ent-DDI, which are more stable than the cyclic lactone NCSi, have been shown to bind to bulged DNA and to be useful probes of the role of bulged structures in DNA. It has been shown that DDI significantly stimulates DNA strand slippage synthesis by DNA polymerase I with a series of primer-template motifs containing different nucleotide repeats (*21*), presumably by binding to bulged intermediates involved in the slippage process. Both diastereomers resemble NCSi-gb in having a high affinity for the two-base bulged DNA duplex and a low affinity for the DNA duplex lacking a bulge base. However, differential binding affinity between the two diastereomers was detected depending on the bulge size and sequence, emphasizing the difference that the stereochemistry imparts (*20*). DDI showed approximately 2 and 5 times greater binding affinity than ent-DDI for two- and single-base bulged DNAs, respectively. In addition, variation of bases adjacent to the bulge residues resulted in different effects on the binding affinities for two agents.

Since the rigid spirocyclic ring connecting BI, NAP, and aminoglycoside has been shown to be a key structure for bulge-specific recognition of DNA, it is expected that its handedness should also be a crucial element in governing the bulge binding in DNA, influencing both the binding mode and the orientation at the bulge site. We have earlier proposed that the right-handedness of the cyclospirolactone connecting THI and NA and carbohydrate units in the NCSi-gb-bulged DNA complex was an important factor that determined its binding orientation in the major groove (*18*). In the complex, the two drug ring systems of NCSi-gb mimic the geometry of the helical bases with a twist angle of ~35° and a rise of ~3 Å at the narrower end, so as to mediate the helical transition between the two half helices on either side of the bulge. Therefore, structural studies of the DNA complexes formed by the spirocyclic enantiomers with opposite handedness are necessary to understand its role in governing the binding affinity and orientation of the enantiomers in the complex.

We have recently elucidated the structure of the complex formed between DDI and a two-base bulged DNA duplex by NMR (*22*). These studies revealed a binding mode that differs from that of the natural product, providing a basis

for understanding the relative binding affinities of the synthetic drug and NCSi-gb for bulges of different sizes and sequences. Herein, we report the elucidation of the structure of the complex formed between ent-DDI and bulged DNA duplex and compare it with that of the DDI-bulged DNA duplex. We show that the enantiomeric aglycone geometry of the two diastereomers leads to different binding modes at the bulge site, and this accounts for their relative binding affinities for various bulges. Further, we find by NMR and CD spectroscopy that significantly different DNA conformational changes occur upon complex formation with the two diastereomers. This analysis provides a rational basis for the design of stereochemically controlled drugs as specific DNA bulge binders.

MATERIALS AND METHODS

Sample Preparation. The synthesis and purification of ent-DDI have been reported (*20*). The oligonucleotide sequences, a 14-mer containing a two-base bulge and its complementary 12-mer (Figure 1D), were synthesized using standard phosphoramidites on an ABI 381A DNA synthesizer. The oligonucleotides were purified by reverse phase HPLC and then desalted with a Sephadex-10 column. The stoichiometry of the duplex formation was verified via titration of the two individual strands above the melting temperature of the duplex, followed by 1-D NMR. The resulting two-base bulge DNA duplex was dissolved in a solution containing 0.1 M NaCl, 10 mM sodium phosphate, and 0.1 mM EDTA (pH 6.5) (NMR buffer). The 1:1 drug−DNA duplex complex was formed by progressively adding microliter aliquots of a 5 mM stock solution of ent-DDI in d_4-MeOH to the DNA duplex and monitoring the titration by 1-D NMR at 25 °C. Formation of the drug−DNA complex was assessed by the disappearance of the resonance lines of the free DNA when ent-DDI was added to the DNA duplex. The complex solution was lyophilized several times and dissolved in 99.96% D_2O. The NMR sample contained a 1:1 ent-DDI-DNA complex at a concentration of ~1.2 mM (pH 6.5).

NMR Experiments. NMR spectra were acquired on Bruker 600 MHz and Varian 500 and 750 MHz spectrometers. NOESY (60, 120, 180, and 250 ms mixing times), DQF−COSY, TOCSY (30 and 80 ms mixing times), and ^{1}H-^{31}P correlation spectra were recorded for the free DNA and the complex in D_2O buffer at 25 °C. Proton NOESY data in H_2O buffer were collected at 1 °C (200 ms mixing time) with the WATERGATE pulse sequence (*23*) for the suppression of the water signal. Proton chemical shifts were referenced to the HOD resonance (4.7 ppm at 25 °C). ^{31}P chemical shifts were referenced relative to an external trimethyl phosphate in an aqueous solution containing 0.1 M NaCl (pH 6.5). NMR data were processed using the NMRPipe program (*24*) and analyzed using Sparky version 3.106 (*25*). All resonances in the free duplex and ent-DDI-bulged DNA complex were assigned using standard procedures (*26*).

NMR Restraints. 2-D NOE intensities were determined by the fitting method using a Gaussian function in Sparky version 3.106 (*25*). The interproton distances were derived from the buildup of NOE cross-peak intensities at 60, 120, 180, and 250 ms. Distance ranges of 1.8−2.5, 2.5−3.8, and 3.8−5.5 Å were set for relatively strong, intermediate, and weak NOE cross-peak intensities, respectively. Watson−Crick hydrogen bonding restraints were imposed on the basis of the observed NOEs and chemical shifts of imino protons in the duplex DNA. Standard donor−acceptor atom distances (2.6−3.2 Å) for the hydrogen-bonded atoms in B-DNA were used for all base pairs except the bulge residues. For the two base pairs adjacent to bulge residues, which exhibit a line broadening and upfield chemical shift due to their dynamic flexibility, no hydrogen bonding restraints were applied in the initial stage of the calculation. Dihedral angle restraints for sugar and backbone torsion angles were obtained from combined analyses of the DQF−COSY and ^{1}H-^{31}P COSY spectra. All of the residues in the DNA duplex except bulge residues were in the C2′-endo family. For these residues, $^3J_{H1'-H2'}$ was greater than $^3J_{H1'-H2''}$ in combination with absent or very weak H2″-H3′ and H3′-H4′ cross-peaks. Therefore, these residues were restrained at a δ of 150 ± 20 (*27*, *28*). No sugar angle restraints were applied in the initial stage of the calculation to the A6, G7, T8, A20, and T21 residues since most of their COSY cross-peaks were relatively weak in intensity due to line width broadening associated with local motion in the bulge-containing region. The glycosidic torsion angle χ was constrained on the basis of the examination of the H8/H6−H1′/H2′/H3′ distances derived from the 2-D NOE spectra (*29*, *30*). The γ angles of all residues except bulge residues were restrained within the gauche+ (g+) conformation (60 ± 20) since the cross-peaks between H6/H8 and H5′/H5″ protons were weaker than those between H6/H8 and H1′ protons in the short mixing time (60 and 120 ms) NOESY spectra (*27*). The β torsion angles were constrained within the trans (t) conformation (−150 ± 20), based on a qualitative interpretation of J coupling data using the long-range nP−nH4′ four-bond coupling. Further restriction of torsion angles β and γ was achieved by the inspection of line widths of the H4′, H5′, and H5″ proton resonances (*27*). The ϵ angle was constrained by the measurement of the heteronuclear $^3J_{H3'-P}$ coupling constants and the observation that no long-range $^4J_{H2'-P}$ was found in the ^{1}H-^{31}P correlation spectrum (*31*). Additionally, the α and ζ torsion angles were restrained on the basis of the observation of the ^{31}P chemical shifts (*32*).

Structure Calculation. A starting model of the two-base bulged DNA duplex was generated in a β-helical conformation using InsightII (Accelrys Inc.). For a starting model of ent-DDI, the aglycone part was built from X-ray coordinates (*20*), and then the aminoglycoside sugar moiety was attached on the spirocyclic alcohol using InsightII. Bad contacts in each molecule were independently removed by conjugate gradient energy minimization without any NMR restraints. The drug was placed more than 8 Å outside the minor groove of the DNA duplex with its orientation relative to the DNA duplex defined by the available intermolecular restraints in the complex.

Structure calculations were performed with distance geometry and simulated annealing protocols within CNS 1.0 (*33*). Calculation methods followed what was described previously (*22*). The selected DG structures were subjected to restrained molecular dynamics refinement using the simulated annealing protocol. The structures were heated to 1000 K for 40 ps and then cooled over the course of 25 ps to 300 K. During this calculation, the force constants were 50 kcal mol^{-1} Å^{-2} for experimental distance restraints, 200

kcal mol^{-1} rad^{-2} for dihedral restraints, and 4.0 kcal mol^{-1} Å^{-4} for the van der Waals repulsion term. The structures were refined using 200 steps of restrained energy minimization with NOE and dihedral force constants of 75 kcal mol^{-1} Å^{-2} and 200 kcal mol^{-1} rad^{-2}, respectively. Acceptance criteria of converged structures were low overall energies and no significant NOE (>0.2 Å) or dihedral (>5 Å) violation. Final structures were analyzed using CNS to measure the rmsd between an average structure and the converged structure. The helical parameters of the DNA duplex in the complex were characterized using CURVES version 5.1 (*34*).

CD Experiments. CD spectra were recorded on a Jasc-710 spectropolarimeter using 1 cm cuvettes. Data were recorded at a bandwidth of 1.0 nm over a range of 215−315 nm at 25 °C. Conformation of bulged DNA bound drug was obtained by subtracting the drug-only CD signal from that of the complex.

RESULTS

Complex Formation. The dissociation constants (K_d) of DDI and ent-DDI to the two-base bulge DNA duplex in 10 mM phosphate buffer (pH 6.5) were determined by fluorescence quenching of the drug upon DNA binding (Figure S1, Supporting Information). The bulge-containing oligomer binds ent-DDI with a somewhat lower binding affinity (K_d = 5.33 ± 0.30 μM) than that for DDI (K_d = 2.54 ± 0.21 μM).

The binding of ent-DDI to the two-base bulge-containing DNA duplex (bulged DNA duplex) was monitored by 1-D NMR spectroscopy. Figure S2 (Supporting Information) shows 1-D ^{1}H NMR spectra of the bulged DNA duplex, both free and in the presence of 1 equiv of ent-DDI, in D_2O buffer at 25 °C. Only one major oligomers' set of proton resonances was observed, indicating the formation of a unique complex. The formation of the ent-DDI-bulged DNA complex is indicated by the changes in the chemical shifts of the protons of several residues upon addition of the drug. This is particularly apparent for those protons that are on either bulge residues or adjacent to them, such as the methyl protons of T8, T9, and T21 (Figure S2, Supporting Information).

NMR Analysis of Bulged DNA. Figure 2 shows the imino region of exchangeable proton spectra of the ent-DDI-bulged DNA complex in 10% D_2O/90%H_2O buffer collected at 1 °C. The hydrogen-bonded imino protons within base-paired regions resonate between 12 and 14 ppm, whereas the imino protons of the unpaired thymine and guanine at the bulge site resonate at ∼11 ppm. Each thymine imino proton exhibits an NOE cross-peak to the adenine H2 proton across the A·T base pair. However, whereas the thymine imino protons of T16 and T25 exhibit strong NOEs to their corresponding adenine H2 pairs, those of T9 and T21 show observable NOEs to the A20 and A6 adenine H2 pairs, respectively, in the low-contour plot. Such broad imino protons of T9 and T21 indicate that the A·T base pairs adjacent to the bulge bases experience a fast exchange due to the flexibility of base pairing adjacent to the bulge site. Similarly, each guanine imino proton displayed NOE cross-peaks to the hydrogen-bonded and exposed amino protons of their partner cytosine within G·C base pairs (Figure 2). The upfield-shifted imino protons at ∼11 ppm are assigned

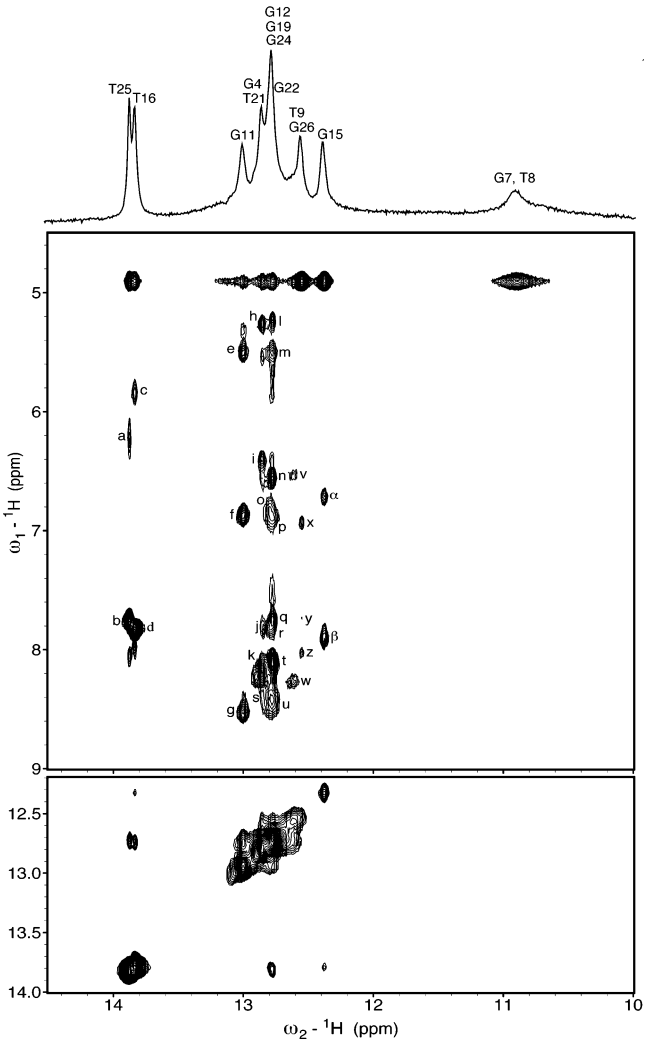

FIGURE 2: Expanded plot of the NOESY (200 ms mixing time) spectrum showing NOE connectivities between the imino protons and the amino protons and between the imino protons for the ent-DDI-bulged DNA complex in H_2O buffer, pH 6.5, at 1 °C. Assignments of the imino protons are labeled at the top of the spectrum. Peaks labeled a−z and α−β are assigned as follows: (a) A2NH_2-T25NH; (b) A2H2-T25NH; (c) A13NH_2-T16NH; (d) A13H2-T16NH; (e) C18H5-G11NH; (f) C18NH_2[e]-G11NH; (g) C18NH_2[b]-G11NH; (h) C23H5-G4NH; (i) C23NH_2[e]-G4NH; (j) A6H2-T21NH; (k) C23NH_2[b]-G4NH; (l); C3H5-G24NH (m) C17H5-G12NH; (n) C3NH_2[e]-G24NH; (o) C17NH_2[e]-G12NH; (p) C10NH_2[e]-G19NH; (q) A2H2-G24NH; (r) A13H2-G12NH; (s) C17NH_2[b]-G12NH; (t) C3NH_2[b]-G24NH; (u) C10NH_2[b]-G19NH; (v) C5NH_2[e]-G22NH; (w) C5NH_2[b]-G22NH; (x) C1NH_2[e]-G26NH; (y) A20H2-T9NH; (z) C1NH_2[b]-G26NH; (α) C14NH_2[e]-G15NH; and (β) C14NH_2[b]-G15NH. The symbols "b" and "e" refer to the hydrogen-bonded and exposed cytosine amino protons, respectively, involved in Watson−Crick base pairing.

to bulge residues. No NOEs were detected between the imino proton of the bulge residues and the other amino and nonexchangeable protons in the NOESY contour plots of the complex due to a rapid exchange with solvent. The chemical shifts of the exchangeable protons are listed in Table S1 of the Supporting Information.

The expanded NOESY (250 ms mixing time) contour plot establishing sequential connectivities between the base protons (7.0−8.4 ppm) and the sugar H1′ and cytosine H5 protons (5.2−6.4 ppm) of the ent-DDI-bulged DNA complex is given in Figure 3. The base to sugar H1′ proton connectivities are traced from C1 to C14 along the bulge-

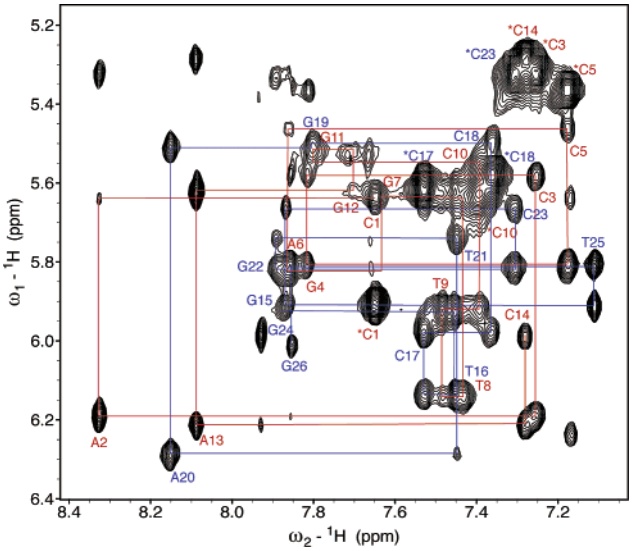

FIGURE 3: Expanded plot of the NOESY (250 ms mixing time) spectrum of the ent-DDI-bulged DNA complex in D_2O buffer, pH 6.5, at 25 °C. The red and blue lines represent the H1′-H6/H8 sequential connectivities for the bulge-containing strand of C1−C14 and the complementary strand of G15−G26, respectively. Asterisks indicate cytosine H6−H5 cross-peaks.

containing strand (Figure 3, red line) and from G15 to G26 along the complementary strand (Figure 3, blue line). The overall pattern of NOE cross-peaks and relative intensities is consistent with a right-handed double helix and a glycoside torsion angle in the anti range for the complex. The interruptions in the sequential connectivities were detected at the A6-G7 and G7-T8 steps. Also, very weak NOE cross-peaks were observed between C5 H1′ and A6 H8 and between T8 H1′ and T9 H6. In addition, an unusually strong NOE peak was detected for T8 H1′−T9 CH3 cross-peak. These data indicate that both of the unpaired bases, G7 and T8, are at the extrahelical position. In the complementary strand, T21 H6 exhibited a weak sequential NOE cross-peak to A20 H1′, and T21 CH_3 exhibited an unusually strong NOE cross-peak to A20 H3′. Numerous changes in chemical shift are observed for the nonexchangeable protons in the ent-DDI-bulged DNA complex, relative to the free bulge DNA duplex (Figure 4A,B). Upfield chemical shifts are observed for the protons of A6 and G7 in the bulge-containing strand. Further, significant downfield shifts are observed for protons of G7, T8, T9, A20, and T21 in both strands. Consequently, the resonances of A6, G7, T8, and T9 of the bulge-containing strand and A20 and T21 of the complementary strand exhibit modest to large chemical shift changes upon complex formation, indicating that such perturbations are localized near the bulge site. It should be noted that the protons of the DNA residues that are subjected to chemical shift changes by the binding of ent-DDI are identical to those by binding of DDI, but the magnitudes of the chemical shift changes for the ent-DDI-bulged DNA are smaller than those for the DDI-bulged DNA duplex, indicating that ent-DDI binds to the same bulge site of the DNA duplex as does DDI but is associated with different conformational changes in the DNA upon complex formation. The chemical shifts of the nonexchangeable protons are listed in Table S2 of the Supporting Information.

The proton-decoupled phosphorus spectrum of the complex has been recorded in D_2O buffer at pH 6.5 and 25 °C.

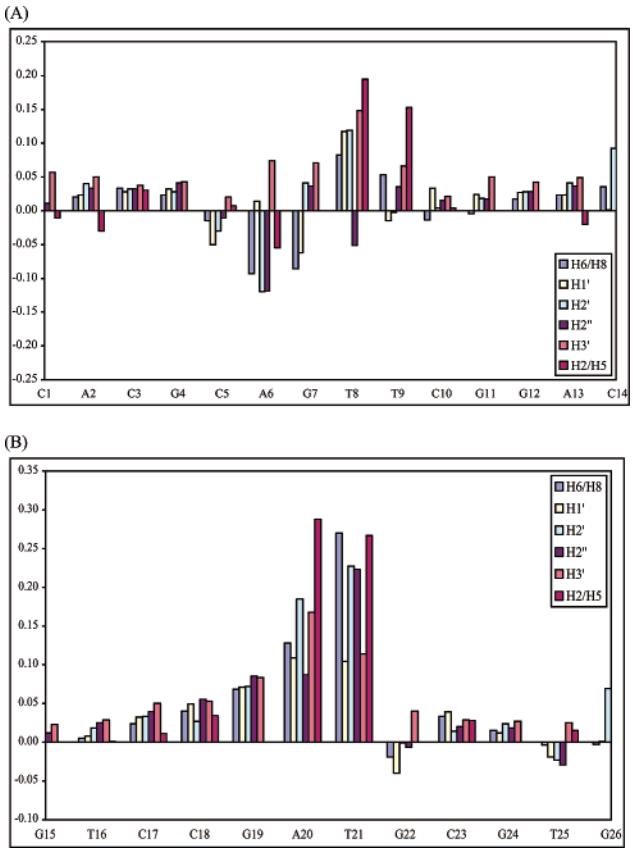

FIGURE 4: Changes in chemical shift for oligonucleotides of the ent-DDI-bulged DNA complex relative to the free DNA duplex. Positive values of $\Delta\delta$ represent downfield chemical shift changes. (A) DNA residues in the bulge-containing strand; (B) DNA residues in the complementary strand.

The phosphorus resonances are dispersed over a 1.0 ppm range between −3.5 and −4.5 ppm and have been assigned from an analysis of the proton-detected phosphorus-proton heteronuclear correlation experiment with the expanded contour plot shown in Figure S3 (Supporting Information). The phosphorus resonances for the free DNA duplex and the complex and their chemical shift difference are given in Table S3 of the Supporting Information. The ^{31}P resonances of A6, T8, and T9 are upfield-shifted, and the ^{31}P resonances of A20 and T21 are downfield-shifted upon complex formation. This perturbation in ^{31}P chemical shifts is in accord with chemical shift changes of proton resonances on complex formation.

NMR Analysis of ent-DDI in the Complex. The NMR spectra of free ent-DDI in CD_3OD were previously characterized for complete chemical shift assignment and structural conformation (*20*). All proton resonances of DNA-bound ent-DDI were assigned in a manner similar to that described for the assignments of the free ent-DDI. The chemical shifts for ent-DDI, both free in an aqueous solution and when bound to the bulge DNA duplex, are shown in Table S4 of the Supporting Information. Proton resonances of ent-DDI in the complex were restricted to only one set, exhibiting spin connectivities and characteristic intramolecular NOEs similar to those of the free ent-DDI. Ent-DDI in the bound form exhibits a strong H25−H1 NOE cross-peak and medium H11−H6 and H22−H6 NOE cross-peaks, which are characteristic NOEs between spirocyclic aglycone protons and are similar to those for the DDI-bulged DNA complex.

Table 1: Intermolecular NOEs Observed between Ent-DDI and DNA Protons

Ent-DDI	DNA contacts
H1	A20H2
H2	A20H2
H3	G7H1′, T8H4′, T8H5″, T9H6, T9CH$_3$
H4	G7H1′, T8H4′, T8H5″, T9H4′, T9TH5″
H6a, H6b	G7H4′
H12	T21H1′, G22H5″
H17	A6H2
H18	A6H2, A6H8
H19	A6H1′, A6H2″, A6H2′, A6H8, G7H1′, G7H8
H20	A6H1′, A6H2″, A6H8, G7H6, G7H4′, G7H5″
H22	G7H4′
H24a, 24b	A20 H1′, T21 H4′, T21H5″
H25	A20H2
H1′	A20H2
H3′	A20H2, C10 H1′, C10 H4′
H5′	A20H2
H6′, H6″	A20 H1′, T21H4′

The ent-DDI-bulged DNA complex has strong/medium H1′−H25/H1 NOE cross-peaks and weak/medium H5′−H24 and H1′/H2′−H7 NOE cross-peaks, which are interresidue NOEs between aglycone and aminoglycoside protons and different from those for the DDI-bulged DNA complex. The chemical shift differences of ent-DDI between the free and the complexed forms are shown in Figure S4 (Supporting Information). The resonances of the aglycone protons in the ent-DDI-bulged complex are upfield-shifted in the large to modest (0.2−0.6 ppm) range as compared to those of free ent-DDI, whereas resonances of the aminoglycoside protons are mostly downfield-shifted. The majority of BI ring protons exhibit larger chemical shift changes as compared to the NAP ring protons, indicating the intercalation by the BI upon complex formation. However, the upfield shift of the BI moiety in the ent-DDI-bulged complex is much smaller than those in the DDI-bulged complex, demonstrating that intercalation of the BI moiety in the ent-DDI-bulged DNA complex is not as extensive as in the DDI-bulged DNA complex.

Intermolecular NOEs in the Complex. A number of intermolecular NOEs between the bulged DNA duplex and the ent-DDI protons have been identified and assigned for the ent-DDI-bulged DNA complex. The largest numbers of intermolecular NOEs are identified between the two aromatic ring protons of ent-DDI and the A6-G7-T8-T9 sequence of the bulge-containing strand, indicating that the two aromatic rings of ent-DDI are positioned toward the bulge region. It is readily apparent that most of the components of the ent-DDI show extensive NOEs to primarily the DNA minor groove protons. These intermolecular NOEs are listed by residue position within each component of the complex in Table 1 and provide critical restraints for aligning the DDI on the DNA and defining the solution structure of the complex.

The distribution of the observed intermolecular NOEs readily provides insights into the alignment of the ent-DDI in the complex. Most protons of the BI moiety show NOEs to the base and sugar protons of A6, and H19 and H20 protons of the distal edge of the BI ring system exhibit NOEs to the protons of G7 (Table 1). Also, the H12 proton of the other short edge of the BI moiety shows NOEs to the H1′ proton of T21 (Figure S5, Supporting Information). These

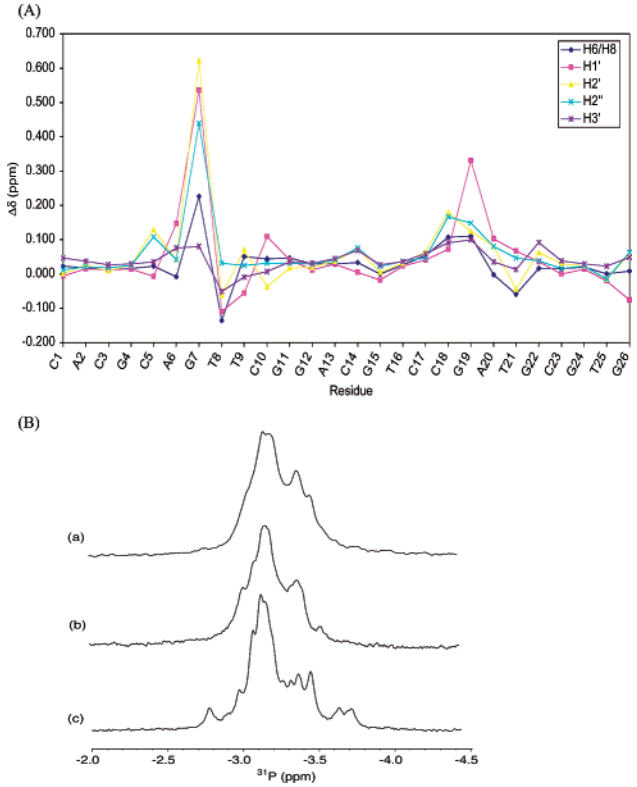

FIGURE 5: (A) Chemical shift differences between the DDI- and the ent-DDI-bulged DNA complex. $\Delta\delta$ is the value resulting when the DNA proton chemical shifts of the DDI-bulged DNA complex are subtracted from those of the ent-DDI-bulged DNA complex. (B) 1-D phosphorus spectra of (a) free bulged duplex, (b) ent-DDI-bulged DNA complex, and (c) DDI-bulged DNA complex.

NOE patterns suggest that the BI ring system is intercalated below A6·T21, and its distal edge faces toward the G7 bulge base. The NAP moiety, the other ring system of ent-DDI, exhibits several NOEs to minor groove sugar protons (H1′ and H4′) of G7, T8 of the bulge-containing strand, and H2 proton of A20 of the complementary strand, establishing that the NAP moiety is positioned in the minor groove of the G7−T8−T9 bulge site. The aminoglycoside sugar ring is also positioned in the minor groove on the basis of the observed NOEs between the aminoglycoside protons and the H2 proton of A20. Additionally, the H24 protons of the spirocyclic ring exhibit NOEs to H1′ of A20 and H4′ of T21, providing evidence for binding from the minor groove. Thus, all of the intermolecular NOEs suggest that the BI moiety is intercalated below the A6·T21 base pair, while the NAP and aminoglycoside moieties remain in the minor groove at the site of the bulge pocket and adjacent to the T9·A20 base pair, respectively.

Comparison of DDI- and ent-DDI-Bulged DNA Complex by NMR. Figure 5A shows chemical shift differences for the oligonucleotides between the DDI- and the ent-DDI-bulged DNA complexes. A striking difference is observed at the G7 residue, one of unpaired bases, indicating its different placement in the helical duplex. The G7 in the DDI-bulged DNA complex stacks inside the helix, whereas that in the ent-DDI bulged DNA complex is at an extrahelical position. In addition, modest chemical shift differences are detected at the residues adjacent to the bulge site, suggesting that structural perturbations of the DNA residues at the bulge site upon complex formation are different for the two

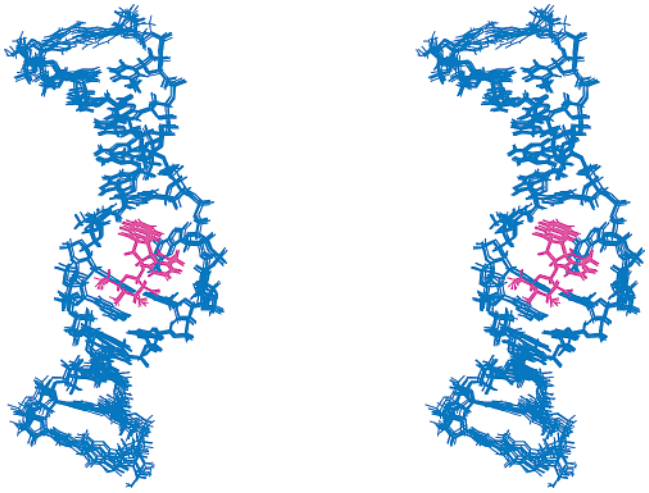

FIGURE 6: Stereoview of the superimposed final 10 structures by simulated annealing for the ent-DDI-bulged DNA complex viewed from the minor groove. The DNA and drug are shown in blue and pink, respectively.

complexes. 1-D ^{31}P spectra at 25 °C for the free bulged DNA duplex, ent-DDI-bulged DNA complex, and DDI-bulged DNA complex are shown in Figure 5B. Comparison of ^{31}P chemical shift dispersion for the three DNA duplexes shows that the DNA backbone conformation of the ent-DDI-bulged DNA complex is similar to that of the free DNA duplex but differs from that of the DDI-bulged DNA complex, indicating that the ent-DDI-bulged DNA complex does not undergo a significant conformational change. Also, this result is in accord with the smaller proton chemical shifts in the ent-DDI-bulged DNA complex as compared with those in the DDI-bulged DNA complex.

Structure Calculation. Forty-two DNA−drug intermolecular NOEs provide information about the binding site of the drug. NMR results were incorporated as initial distance and dihedral angle restraints in the structure calculation. The structure computation was carried out in an iterative manner in which distances derived from the calculated structures were compared with the experimental data. On the basis of these analyses, distance bounds and NOE force constants of various groups of NOE restraints were adjusted, and a new generation of structures was calculated using the newly modified protocol. The final structures were selected on the basis of criteria such as low overall energies and no significant NOE (>0.2 Å) and dihedral (>5 Å) violations. Ten superimposed structures are presented as the final results in Figure 6. The final refined structures converged to a pairwise rms difference of 0.54 and very low constraint violation energies (Table 2). These converged structures show good bond and angle geometry, and in general, satisfy NMR-derived distances and dihedral angles.

Elucidation of the Structure of the Ent-DDI-Bulged DNA Complex. The BI moiety is intercalated from the minor groove, while the NAP and aminoglycoside moieties are positioned in the minor groove. Intercalation of the BI moiety between A6·T21 and T9·A20 base pairs in the complex is shown on the right in Figure 7A as a view normal to the helix. The BI ring plane tilts diagonally with respect to the A6·T21 base pair and stacks above the purine ring of A20. The distal edge of the BI ring moiety proceeds toward the purine ring of G7. Thus, the BI ring moiety is surrounded by G7-A6·T21-A20, consisting of the one unpaired base and the three bases adjacent to the bulge site. The approach of the NAP moiety toward the bulge region of the minor groove and the positioning of the sugar ring in the middle of the minor groove in the ent-DDI-bulged DNA complex are shown on the right in Figure 7B. The NAP moiety is positioned in the minor groove along the G7-T8-T9 bulge pocket. The distal edge of the NAP ring moiety faces toward the purine ring of A20. The aminoglycoside moiety is located in the minor groove near the A20 residue.

Table 2: Structural Statistics for 10 Refined Structures of the Ent-DDI-Bulged DNA Complex

NOE distance restraints	427
intraresidue (DNA)	168
interesidue (DNA)	139
hydrogen Bond (DNA)	32
intraresidue (ent-DDI)	46
intermolecular (ent-DDI-DNA)	42
dihedral restraints	166
average NOE violations (>0.20 Å)	0
average dihedral angle violation (>5°)	0
pairwise rmsd for all heavy atoms (Å)	0.548 ± 0.216
mean deviation from covalent geometry	
bond lengths (Å)	0.0036 ± 0.00001
bond angles (deg)	0.5385 ± 0.0042
impropers (deg)	0.4866 ± 0.0006

CD Studies of Conformations of Drug−DNA Complexes. Figure 8 shows the CD spectra of the free DNA and its altered DNAs after subtracting the drug-alone spectrum from the complexes, assuming that the conformation of the drug is not significantly altered since the aglycone structures of two DDI diastereomers are relatively rigid. The CD spectrum of DNA for the DDI-bulged DNA complex as compared to that of the native DNA was more significantly changed than that for the ent-DDI-bulged DNA complex. The DNA curve for the DDI-bulged DNA complex exhibits significant red shifts of both the positive and the negative bands and greater negative ellipticity change upon complex formation, indicating that the DNA in the DDI-bulged DNA complex undergoes larger conformational changes, resulting in better drug binding as compared to the ent-DDI-bulged DNA complex (*35*). The ent-DDI-bulged DNA complex shows modest ellipticity decreases in the positive and negative bands and no band shifts. These distinct differences for the DNAs complexed with the two diastereomers suggest that the structural perturbations in the DNA upon drug binding differ significantly with the diastereomeric drugs. This result is consistent with the NMR data showing that chemical shift differences of the ent-DDI-bulged-DNA complex as compared to free DNA are smaller than that of the DDI-bulged DNA complex and serves to explain why the ent-DDI shows a lower binding affinity for the two base-bulged DNA.

DISCUSSION

Fluorescence quenching studies have identified a two-base bulge in DNA as the preferred binding site for both DDI and ent-DDI (*20*). The overall binding specificity of DDI for two-base bulge-containing oligonucleotides are ~2-fold greater than that of the ent-DDI. In each case, NMR studies reveal a unique structure of the drug−DNA complex with drug binding limited to the bulge site. This is evident from the NOE cross-peaks observed between the drugs and the

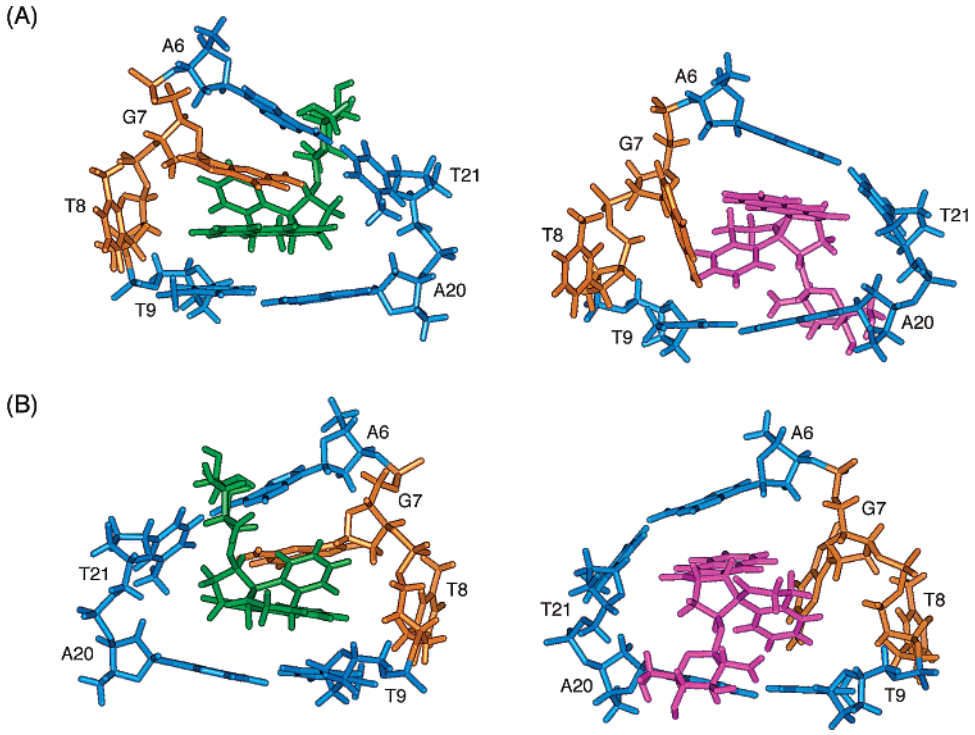

FIGURE 7: Stick view of the binding site in the DDI-bulged DNA complex (left) and ent-DDI-bulged DNA complex (right) looking into the major (A) and minor (B) grooves. The two base pairs and two bulge bases are shown in blue and orange, respectively. DDI and ent-DDI are shown in green and pink, respectively.

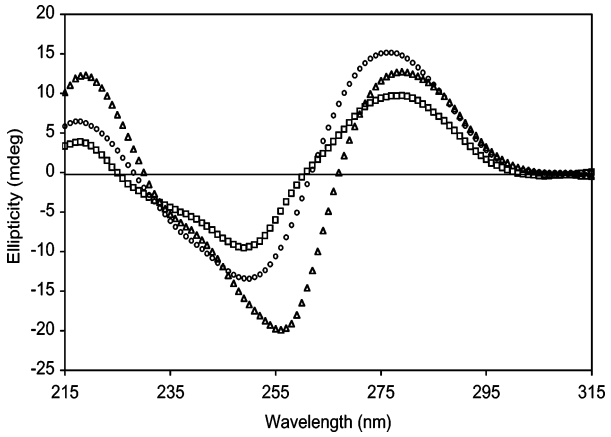

FIGURE 8: CD spectra of free DNA (○), DDI-bulged DNA duplex (△), and ent-DDI-bulged DNA complex (□).

oligonucleotide protons, which surround the bulge region. A higher affinity for the bulge region is consistent with the binding results of the natural product, despite the differences in details of the binding mode.

The BI moiety of ent-DDI intercalates between the A6·T21 and the T9·A20 base pairs, overlapping with portions of the purine bases, while the NAP moiety is positioned in the minor groove along the G7−T8−T9 bulge sequence to which the NAP ring protons show NOE interactions. The aminoglycoside is in the middle of the minor groove, approaching A20 of the nonbulged strand. In accordance with the NOEs described previously, the distal edge of the BI aromatic ring system faces toward the G7 bulge base, whereas the other end of the ring remains at the T21 residue. This orientation of ent-DDI to the DNA duplex is totally different from that of DDI, where the BI moiety of DDI intercalates into the G7−T8−T9·A20 pocket, and the aminoglycoside is positioned in the minor groove near the T21 residue of the nonbulged strand. These data demonstrate that the alignment of ent-DDI along the DNA helical duplex is in the reverse direction to that of DDI (Figure 7A,B).

Both the DDI and the ent-DDI diastereomers bind in the minor groove with a preference for the bulge region. However, there are several clear differences in the details of their binding characteristics. First, the DDI shows a stronger affinity for the two-bulge sequence than does ent-DDI. This is clearly derived from the NMR and CD data, showing that the DNA in the DDI-bulged DNA complex undergoes a larger conformational change upon complex formation in comparison to the ent-DDI-bulged DNA complex. Second, the chemical shift changes of the DNA protons at the binding site in the presence of DDI are different from ent-DDI. The striking chemical shift difference between the two complexes is observed at the G7 bulge residue, indicating its different position in the helical duplex. Also, modest, but significant, chemical shift differences between the complexes are detected at most of the residues of the bulge region, suggesting that structural perturbation at the bulge site upon complex formation is different for the two complexes. The extrahelical position preference of both bulge bases in the ent-DDI bulged DNA complex may account for the finding that ent-DDI showed a much lower binding affinity for a single-base bulge site than for a two-base bulge site in the DNA duplex as compared to DDI (*20*). Third, the DNA protons for which NOE interactions are observed in the two complexes are derived from the same residues at the bulge binding site, but the NOE connections between the DNA and the drug protons are totally different for the two agents, consistent with the difference in the bind-

ing modes preferred by the two diastereomers. The most striking difference between the two diastereomers, however, is their reverse binding orientation. The aminoglycoside moiety of the ent-DDI is positioned in the 3′ direction from the bulge region, whereas the sugar of DDI is positioned in the 5′ direction from the same site. It is notable that the reverse binding orientation within the bulge site is the natural consequence of the opposite handedness imposed by the spirocyclic ring junction and permits the two aromatic ring systems of the spirocyclic enantiomers access to the bulge region.

These structural studies with the spirocyclic enantiomers clearly demonstrate that the two-base bulge in duplex DNA provides an optimal binding site for wedge-shaped molecules in which the two aromatic ring moieties are fixed in relation to each other by the rigid spirocyclic structure. The opposite handedness of the spirocyclic enantiomers requires that they bind to the bulge site with reverse orientations in the helical axis. In each case, however, the BI moiety is intercalated into the helix, and the NAP and aminoglycoside moieties are positioned in the bulge region and the middle of the minor grove, respectively. Thus, it is apparent that the binding mode and orientations of the opposite handed, wedge-shaped molecules in the DNA are determined by the requirement that the two aromatic ring systems fit into the pocket at the bulge site. However, the reverse binding orientations of the two spirocyclic enantiomers result in different DNA conformational changes and placement of the bulge bases within the helix, likely accounting for their different binding affinities in relation to bulge sequence and size.

Comparative 3-D models of the DDI and ent-DDI-bulged DNA complexes illustrate that the simple event governing complex formation is the accessibility of the aromatic ring moieties of the drugs to bulge sites that have sufficient room to accommodate rigid spirocyclic structures. This necessitates reverse orientation of the two diastereomers for bulge binding. Elucidation of the structures of the two complexes provides a basis for understanding the relative binding affinities of the spirocyclic enantiomers and for the role of stereochemical factors in determining the precise mode of binding. Such detailed information on the location and orientation of stereospecific agents when bound to targeted sites in DNA is essential to proceed with informed structural design of agents with a high affinity for bulged sites in DNA (and RNA). Finally, these studies place additional emphasis on the importance of the precise site of placement of the aminoglycoside moiety on the drug in determining the mode of approach of the wedge to the bulge site. Unlike the natural product, both spirocyclic enantiomers, which have the sugar unit attached to the spirocyclic oxygen, are minor groove specific agents. To fully explore the role of the site of aminosugar conjugation in determining groove specificity, we are in the process of synthesizing spirocyclic agent analogues with the sugar attached to the other available oxygens of the NAP and BI moieties.

ACKNOWLEDGMENT

We appreciate the availability of NMR time provided at the Harvard Medical School. We thank X. Gao (University of Houston) for discussion of the binding mode and allowing us to use the NMR facility funded by the W. M. Keck Foundation in our initial experiments. We thank F. S. Fouad and Z. Xi for the chemical synthesis of the spirocyclic compounds.

SUPPORTING INFORMATION AVAILABLE

Chemical shift assignments for the exchangeable protons of the ent-DDI-bulged DNA complex (Table S1) and the nonexchangeable protons of the ent-DDI-bulged DNA complex (Table S2), chemical shift assignments of the phosphorus resonances and their differences of the bulged DNA in the complex and in the free form (Table S3), ^{1}H NMR chemical shifts of ent-DDI in the free and complex forms (Table S4), fluorescence quenching of DDI and ent-DDI by the bulged DNA duplex (Figure S1), ^{1}H NMR spectra of (A) free bulged DNA duplex and (B) the 1:1 complex of ent-DDI-bulged DNA duplex in D_2O (Figure S2), changes in chemical shift for bound ent-DDI relative to the free ent-DDI (Figure S3), contour plot of the proton detected ^{1}H-^{31}P correlation spectrum of the ent-DDI-bulged DNA complex (Figure S4), expanded region of the NOESY spectrum showing the intramolecular and intermolecular cross-peaks of ent-DDI (Figure S5), space-filling view looking into the minor groove (A) and van der Waals surface at the binding site (B) of the ent-DDI-bulged DNA complex (Figure S6). This material is available free of charge via the Internet at http://pubs.acs.org.

REFERENCES

1. Degtyareva, N., Subramanian, D., and Griffith, J. D. (2001) Analysis of the binding of p53 to DNAs containing mismatched and bulged bases, *J. Biol. Chem. 276*, 8778−8784.
2. Payet, D., Hillisch, A., Lowe, N., Diekmann, S., and Travers, A. (1999) The recognition of distorted DNA structures by HMG-D: a footprinting and molecular modelling study, *J. Mol. Biol. 294*, 79−91.
3. Wang, Y.-H., Bortner, C. D., and Griffith, J. (1993) RecA binding to bulge- and mismatch-containing DNAs, *J. Biol. Chem. 268*, 17571−17577.
4. Nelson, J. W., and Tinoco, I. (1985) Ethidium ion binds more strongly to a DNA double helix with a bulged cytosine than to a regular double helix, *Biochemistry 24*, 6416−6421.
5. Nakatani, K., Sando, S., and Saito, I. (2000) Recognition of a single guanine bulge by 2-acylamino-1,8-naphthyridine, *J. Am. Chem. Soc. 122*, 2172−2177.
6. Colgrave, M. L., Williams, H. E. L., and Searle, M. S. (2002) Structure of a drug-induced DNA T-bulge: Implications for DNA frameshift mutations, *Angew. Chem., Int. Ed. 41*, 4754−4756.
7. Williams, L. D., and Goldberg, I. H. (1988) Selective strand scission by intercalating drugs at DNA bulges, *Biochemistry 27*, 3004−3011.
8. Kappen, L. S., and Goldberg, I. H. (1993) Site-specific cleavage at a DNA bulge by neocarzinostatin chromophore via a novel mechanism, *Biochemistry 32*, 13138−13145.
9. Xi, Z., Mao, Q. K., and Goldberg, I. H. (1999) Mechanistic studies on the base-catalyzed transformation of neocarzinostatin chromophore: Roles of bulged DNA, *Biochemistry 38*, 4342−4354.
10. Nakatani, K., Okamoto, A., and Saito, I. (1999) Specific alkylation of guanine opposite to a single nucleotide bulge: A chemical probe for the bulged structure of DNA, *Angew. Chem., Int. Ed. 38*, 3378−3381.
11. Hamy, F., Felder, E. R., Heizmann, G., Lazdins, J., Aboul-ela, F., Varani, G., Karn, J., and Klimkait, T. (1997) An inhibitor of the Tat/TAR RNA interaction that effectively suppresses HIV-1 replication, *Proc. Natl. Acad, Sci. U.S.A. 94*, 3548−3553.
12. Kappen, L. S., and Goldberg, I. H. (1995) Bulge-specific cleavage in transactivation response region RNA and its DNA analogue by neocarzinostatin chromophore, *Biochemistry 34*, 5997−6002.

13. Xi, Z., and Goldberg, I. H. (1999) DNA-Damaging Enediyne Compounds, in *Comprehensive Natural Products Chemistry* (Barton, D. H. R., Nakanishi, K., and Meth-Cohn, O., Eds.) Vol 7, pp 553−592, Elsevier Science, Oxford.
14. Kappen, L. S., and Goldberg, I. H. (1993) DNA conformation-induced activation of an enediyne for site-specific cleavage, *Science 261*, 1319−1321.
15. Hensens, O. D., Chin, D.-H., Stassinopoulos, A, Zink, D. L., Kappen, L. S., and Goldberg, I. H. (1994) Spontaneous generation of a biradical species of neocarzinostatin chromophore: role in DNA bulge-specific cleavage, *Proc. Natl. Acad. Sci. U.S.A. 91*, 4534−4538.
16. Yang, C. F., Stassinopoulos, A., and Goldberg, I. H. (1995) Specific binding of the biradical analogue of neocarzinostatin chromophore to bulged DNA: implications for thiol-independent cleavage, *Biochemistry 34*, 2267−2275.
17. Stassinopoulos, A., Ji, J., Gao, S., and Goldberg, I. H. (1996) Solution structure of a two-base DNA bulge complexed with an enediyne cleaving analogue, *Science 272*, 1943−1946.
18. Gao, X., Stassinopolous, A., Ji, J., Kwon, Y., Bare, S., and Goldberg, I. H. (2002) Induced formation of a DNA bulge structure by a molecular wedge ligand-post activated neocarzinostatin chromophore, *Biochemistry 41*, 5131−5143.
19. Xi, Z., Jones, G. B., Qabaja, G., Wright, J. W., Johnson, F. S., and Goldberg, I. H. (1999) Synthesis and DNA binding of spirocyclic model compounds related to the neocarzinostatin chromophore, *Org. Lett. 1*, 1375−1377.
20. Xi, Z., Hwang, G.-S., Goldberg, I. H. Harris, J. L., Pennington, W. T., Fouad, F. S., Qabaja, G., Wright, J. M., and Jones, G. B. (2002) Targeting DNA bulged microenvironments with synthetic agents: Lessons from a natural product, *Chem. Biol. 9*, 925−931.
21. Kappen, L. S., Xi, Z., Jones, G. B., and Goldberg, I. H. (2003) Stimulation of DNA strand slippage synthesis by a bulge binding synthetic agent, *Biochemistry 42*, 2166−2173.
22. Hwang, G.-S., Jones, G. B., and Goldberg, I. H. (2003) Solution structure of a wedge-shaped synthetic molecule at a two-base bulge site in DNA, *Biochemistry 42*, 8472−8483.
23. Piotto, M., Saudek, V., and Sklenar, J. (1992) Gradient-tailored excitation for single-quantum NMR spectroscopy of aqueous solutions, *J. Biomol. NMR 2*, 661−665.
24. Delaglio, F., Grzesiek, S., Vuister, G. W., Zhu, G., Pfeifer, J., and Bax, A. (1995) NMRPipe: a multidimensional spectralprocessing system based on UNIX pipes, *J. Biomol. NMR 6*, 277−293.
25. Goddard, T. D., and Kneller, D. G., *SPARKY 3*, University of California, San Francisco, 2001.
26. Wuthrich, K. (1986) *NMR of Proteins and Nucleic Acids*, pp 224−246 (resonance assignment strategy in nucleic acid) and pp 117−161 (resonance assignment strategy in protein) John Wiley & Sons, New York.
27. Houser, R. V., Ravikumar, M., Chary, K. V. R., Sheth, A., Govil, G., Zu-Kun, T., and Miles, H. T. (1986) Solution structure of d-GAATTCGAATTC by 2-D NMR. A new approach to determination of sugar geometries in DNA segments, *FEBS Lett. 205*, 71−76.
28. Kim, S.-G., Lin, L.-J., and Reid, B. R. (1992) Determination of nucleic acid backbone conformation by ^{1}H NMR, *Biochemistry 31*, 3564−3574.
29. Van Duynhoven, J. P. M., Goudriaan, J., Hilbers, C. W., Wijmenga, S. S. (1992) Quantitative evaluation of TOCSY data. Application to sugar ring conformational analysis, *J. Am. Chem. Soc. 114*, 10055−10056.
30. Rinkel, L., and Altona, C. (1987) Conformational analysis of the deoxyribofuranose ring in DNA by means of sums of proton proton coupling constant: A graphical method, *J. Biomol. Struct. Dyn. 4*, 621−649.
31. Lankhorst, P. P., Haasnoot, C. A., Erkelens, C., and Altona, C. (1984) 1. Carbon-13 NMR in conformational analysis of nucleic acid fragments. 2. A reparametrization of the Karplus equation for vicinal NMR coupling constants in CCOP and HCOP fragments, *J. Biomol. Struct. Dyn. 1*, 1387−1405.
32. Gorenstein, D. G., Schroeder, S. A., Fu, J. M., Metz, J. T., Roongta, V., and Jones, C. R. (1988) Assignments of ^{31}P NMR resonances in oligodeoxyribonucleotides: origin of sequence-specific variations in the deoxyribose phosphate backbone conformation and the ^{31}P chemical shifts of double-helical nucleic acids, *Biochemistry 27*, 7223−7237.
33. Brunger, A. T., Adams, P. D., Clore, G. M., DeLano, W. L., Gros, P., Grosse, K. R., Jiang, J. S., Kuszewski, J., Nilges, M., Pannu, N. S., Read, R. J., Rice, L. M., Simonson, T., and Warren, G. L. (1998) Crystallography and NMR System: A new software suite for macromolecular structure determination, *Acta Crystallogr., Sect. D 54*, 905−921.
34. Program kindly provided by Lavery, R., CNRS Institut de Biologie Physico-Chimique, France. Lavery, R., and Sklenar, H. (1988) The definition of generalized helicoidal parameters and of axis curvature for irregular nucleic acids, *J. Biomol. Struct. Dyn. 6*, 63−91.
35. Yang, C. F., Jackson, P. J., Xi, Z., and Goldberg, I. H. (2002) Recognition of bulged DNA by a neocarzinostatin product via an induced fit mechanism *Bioorg. Med. Chem. 10*, 1329−1335.

BI035824I